International Journal of Thermofluid Science and Technology (2022)
Volume 9, Issue 3, Paper No. 090304
https://doi.org/10.36963/IJTST.2022090304
Research Article

Modeling and simulation of suction-driven flow and heat transfer with temperature-dependent thermal conductivity in a porous channel

Valjacques Nyemb Nsoga, Jacques Hona *

Applied Mechanics Laboratory, Faculty of Science, University of Yaoundé I, P.O. Box 812, Yaoundé, Cameroon

ATICLE INFO

Received: Oct. 20 2021;
Received in revised form:
05 Jan. 2022;
Accepted: 08 Feb. 2022;
Published online:
12 Feb. 2022

Keywords:
Numerical simulation
Nonlinear boundary-value problem
Vorticity transport equation
Heat transfer equation
Suction-driven flow

ABSTRACT

In this paper, the heat transfer equation is coupled to the Navier-Stokes equations for a steady flow induced by uniform suction on two porous walls kept at different temperatures. The incompressibility of the fluid and the fact that the velocity field has two components lead to introduce the stream function in the governing equations. A similarity method is used in order to transform the resulting set of partial differential equations satisfied by the stream function and temperature into two ordinary differential equations for the same problem. The analysis is focused on the description of the behaviors of the normal and axial velocities, the streamlines, and temperature through multiple solution branches under different values of the main control parameters of the problem which are the Reynolds number, the Péclet number and the sensitivity of the thermal conductivity to the variations of temperature.

1. Introduction

The study of heat transfer in fluids and solids is interesting, because many characteristics and physical properties of matter depend on temperature [1-5]. When this heat transfer manifests in a fluid flow, the dependence of the physical properties of the fluid on temperature results in the coupling of the laws that govern the movement of the fluid and the distribution of heat. This coupling can be partial or complete, taking into account the type of the physical property which is sensitive to temperature. Many studies [6-9] consider the variation of the dynamic viscosity or that of the specific mass as a function of temperature. In both cases, the Navier-Stokes equations describing the fluid flow and the heat equation are fully coupled [6-10]. In other words, the solution of one of the equation depends on those of the others. On the other hand, the variation of a property like the thermal conductivity of the fluid as a function of temperature involves a partial coupling, because in this case which is rarely reported in the litterature, only the heat equation needs the solution of the Navier-Stokes equations to be solved, while that heat has no influence on the movement of the ncompressible viscous fluid.

*Corresponding e-mail: honajacques@yahoo.fr (Jacques Hona)

Nomenclature

h	half-width of the channel, m	a^*, b^*	c^* successful initial guesses
T_0	temperature of the cold wall, K	R	Reynolds number
T_1	temperature of the hot wall, K	$Pé$	Péclet number
V	absolute fluid speed at walls, m/s	f	nondimensional function deriving from the integration of the fluid flow equation
c_p	constant pressure specific heat, J/kg.K		
k	temperature-dependent thermal conductivity of the fluid, W/m.K	u, v	numerical functions deriving from the integration of the fluid flow equation
k_0	thermal conductivity at temperature T_0	g, q, w	numerical functions deriving from the integration of the heat transfer equation
x^*	axial coordinate, m		
y^*	normal coordinate, m	G	numerical function to minimize
V_x^*	axial velocity, m/s	m	iteration index
V_y^*	normal velocity, m/s	J	Jacobian matrix
T^*	temperature of the fluid, K	f_1, f_2	numerical functions helping to define the components of the Jacobian matrix
p^*	pressure of the fluid, Pa		
x	nondimensional axial coordinate	*Greek symbols*	
y	nondimensional normal coordinate	γ	nondimensional sensitivity to the thermal conductivity to the temperature variations
V_x	nondimensional axial velocity		
V_y	nondimensional normal velocity	ρ	specific mass of the fluid, kg/m^3
T	nondimensional temperature	μ	dynamic viscosity of the fluid, kg/m.s
p	nondimensional pressure	κ	nondimensional thermal conductivity
F	nondimensional stream function per unit length	θ	nondimensional similarity temperature
		ψ	nondimensional stream function
A	nondimensional axial pressure gradient per unit length	ϕ	nondimensional function deriving from the integration of the heat transfer equation
Q	nondimensional normal pressure gradient	ϕ_1	numerical function helping to define the the components of the Jacobian matrix
a, b,	c input initial guesses		

This is the case which is considered in the current work, where only the energy equation needs the solution of the Navier-Stokes equations to be solved, because of the convection between the velocity field and the gradient of temperature. Due to this convection, the complexity of the Navier-Stokes equations involves that of the heat transfer equation, beacause some terms of the momentum equation deriving from the fluid motion are present in the differential equation describing the evolution of temperature inside the flow domaine. The mathematical model resulting from this coupling becomes very complex, because the problem to solve is equivalent to a single differential equation whose order is equal to the sum of the orders of the Navier-Stokes equations and the heat equation. In addition, the constraints of the equivalent problem represent the sum of the boundary conditions associated with the flow and the heat transfer.

In the present study, a two-dimensional flow driven by suction between two porous walls kept at different temperatures is considered. The heat is transferred from the hot wall to the cold wall and the temperature difference between the two walls causes the variation of the thermal conductivity of the fluid with temperature in a linear law. The approach adopted to solve the problem is based on the similarity method introduced by Berman [11], such that as the flow has two velocity components, notably the axial velocity and the normal velocity, the solution corresponds to the axial velocity depending on the axial and normal Cartesian coordinates that help to build the canal, while the normal velocity depends only on the normal coordinate. This method of solution employed

in the pioneer work of Berman [11] inspired many other studies [12-18], such that the fluid flow between two porous rectangular walls is today called the Berman problem by some authors. Subsequently, the Berman approach was extended to solve several other types of flows, notably the cases where the boundaries of the flow domain are in motion. For this purpose, the movement of the walls can be parallel [19, 20] or transverse [21-23] to the flow. In addition, the similarity solution of the Berman type is also suitable in treating the flow problems in porous cylindrical conduits which may be in motion or stationary [24-26]. The Berman approach is increasingly used and its validity has been tested numerically and experimentally [27, 28]. More precisely, it is a method utilized to investigate many types of flows in cylindrical and Cartesian geometrical configurations.

In light of the previous works cited, in which the general purpose is the analysis of the behavior of the flow field components, it appears that many studies deal with the fluid flows in channels with porous walls. These problems are solved using the Navier-Stokes equations, but the difference from one problem to another is related to the constraints associated with the flow and the type of solution sought. With regard to the constraints, it is important to point out that the Navier-Stokes equations are very sensitive to the boundary conditions and the initial conditions. This is to say for example that, many problems can be formulated by the same differential equation, but the difference at the level of the solutions is mainly related to the boundary conditions. On the other hand, the type of the solution sought is related to the method used to solve the problem. This allows us at this stage, to highlight the particularity of our current study compared to all the previous works cited. Indeed, the novelty of our work is the presentation of the velocity profiles, streamlines and temperature in different solution branches pertaining to a problem of heat transfer with temperature-dependent thermal conductivity coupled to a steady flow. So, this kind of solution has been never reported elsewhere. This type of solution is guided by the introduction of the stream function in the governing equations. In the specific case of our study, it is important to note that the stream function satisfies the vorticity equation because the fluid is incompressible and the velocity field has two components.

Apart from this introduction, the rest of the paper consists of the Section 2 which is devoted to the mathematical formulation of the problem, and the Section 3 that contains the description of the method of integration of the differential equations of the problem, as well as the Section 4 in which the numerical results are presented and discussed. The conclusion intervenes in Section 5.

2. Problem formulation

The incompressible fluid is in motion through a channel that consists of two parallel porous walls fixed at different temperatures and distanced by $2h$ as shown in Fig. 1. The temperature of the cold wall is T_0 and that of the hot wall is T_1. The flow is driven by suction, such that the absolute value of the fluid speed at the porous walls is V. The physical properties of the working fluid are the specific mass ρ, the dynamic viscosity μ, the specific heat at constant pressure c_p, and the temperature-dependent thermal conductivity k which takes the value k_0 at temperature T_0. The channel is built on the basis of a Cartesian coordinate system (x^*, y^*), such that x^* denotes the axial or the longitudinal coordinate. The length of the channel defined along the x^*-axis is very large compared to its width $2h$ defined along the y^*-axis, where y^* denotes the normal or the transversal coordinate. So, this length tends to infinity in order to neglect the influence at the ends in the axial direction. The two-dimensional flow under study is described by two velocity components denoted the axial velocity V_x^* and the normal velocity V_y^*. The variables describing the temperature and pressure inside the channel are T^* and p^*, respectively. In the absence of body forces, due to the fact that the channel is horizontal and by neglecting the dissipation effects that could occur inside the flow domain, the fluid flow and heat transfer in the current configuration are governed by the differential equations as in the following:

$$\frac{\partial V_x^*}{\partial x^*}+\frac{\partial V_y^*}{\partial y^*}=0 \tag{1}$$

$$\rho\left(V_x^*\frac{\partial V_x^*}{\partial x^*}+V_y^*\frac{\partial V_x^*}{\partial y^*}\right)=-\frac{\partial p^*}{\partial x^*}+\mu\left(\frac{\partial^2 V_x^*}{\partial x^{*2}}+\frac{\partial^2 V_x^*}{\partial y^{*2}}\right) \tag{2}$$

$$\rho\left(V_x^*\frac{\partial V_y^*}{\partial x^*}+V_y^*\frac{\partial V_y^*}{\partial y^*}\right)=-\frac{\partial p^*}{\partial y^*}+\mu\left(\frac{\partial^2 V_y^*}{\partial x^{*2}}+\frac{\partial^2 V_y^*}{\partial y^{*2}}\right) \tag{3}$$

$$\rho c_p\left(V_x^*\frac{\partial T^*}{\partial x^*}+V_y^*\frac{\partial T^*}{\partial y^*}\right)=\frac{\partial}{\partial x^*}\left(k\frac{\partial T^*}{\partial x^*}\right)+\frac{\partial}{\partial y^*}\left(k\frac{\partial T^*}{\partial y^*}\right) \tag{4}$$

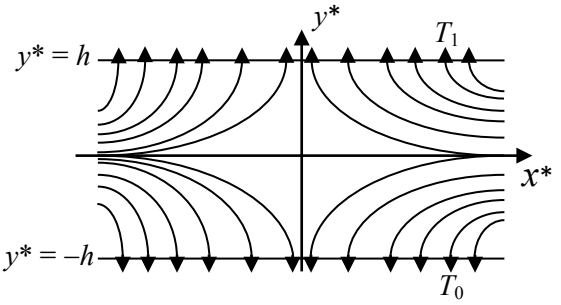

Fig. 1. Geometry of the channel showing the streamlines that represent the flow pattern of a symmetric similarity solution of the Navier–Stokes equations for a suction-driven flow.

The mathematical model of the problem consists of the continuity Eq. (1), the Navier-Stokes Eqs. (2) and (3), as well as the heat transfer Eq. (4). The boundary conditions express the no-slip condition, equal suction speed and the difference of temperatures between the walls:

$$V_x^*=0,\quad V_y^*=V,\quad T^*=T_1 \quad \text{for} \quad y^*=h$$

$$V_x^*=0,\quad V_y^*=-V,\quad T^*=T_0 \quad \text{for} \quad y^*=-h \tag{5}$$

It is convenient at this stage to proceed to the nondimensional formulation of the problem. Indeed, the nondimensional formulation is the removal of units from an equation involving physical quantities. This technique is used in the current work in order to give birth to some control numbers that help in the description of the dynamics of the fluid and the distribution of temperature. In fact, these control numbers are usually provided by using the reference physical quantities for a given problem considering the physical properties of the fluid, the geometry of the flow domain and the boundary conditions. Thus, in this study, the nondimensional variables for length, velocity, temperature and pressure are measured in units of the half-width of the channel h, the fluid suction speed V, the temperature difference between the walls ($T_1 - T_0$) and the reference pressure (ρV^2), respectively. Moreover, the temperature-dependent thermal conductivity is nondimensionalized by its value k_0 at temperature T_0. Hence, the nondimensional variables are defined as follows:

$$x=\frac{x^*}{h},\quad y=\frac{y^*}{h},\quad V_x=\frac{V_x^*}{V},\quad V_y=\frac{V_y^*}{V},$$
$$T=\frac{T^*}{T_1-T_0},\quad p=\frac{p^*}{(\rho V^2)},\quad \kappa=\frac{k}{k_0} \tag{6}$$

In terms of nondimensional variables, the equations describing the problem are derived as in the following:

$$\frac{\partial V_x}{\partial x}+\frac{\partial V_y}{\partial y}=0 \tag{7}$$

$$V_x\frac{\partial V_x}{\partial x}+V_y\frac{\partial V_x}{\partial y}=-\frac{\partial p}{\partial x}+\frac{1}{R}\left(\frac{\partial^2 V_x}{\partial x^2}+\frac{\partial^2 V_x}{\partial y^2}\right) \tag{8}$$

$$V_x\frac{\partial V_y}{\partial x}+V_y\frac{\partial V_y}{\partial y}=-\frac{\partial p}{\partial y}+\frac{1}{R}\left(\frac{\partial^2 V_y}{\partial x^2}+\frac{\partial^2 V_y}{\partial y^2}\right) \tag{9}$$

$$V_x\frac{\partial T}{\partial x}+V_y\frac{\partial T}{\partial y}=\frac{1}{Pé}\left(\frac{\partial}{\partial x}\left(\kappa\frac{\partial T}{\partial x}\right)+\frac{\partial}{\partial y}\left(\kappa\frac{\partial T}{\partial y}\right)\right) \tag{10}$$

where the Reynolds number $R = \rho Vh/\mu$ and the Péclet number $Pé = \rho Vhc_p/k_0$ are introduced. The nondimensional boundary conditions are given by:

$$V_x = 0, \quad V_y = 1, \quad T = \frac{T_1}{T_1 - T_0} \quad \text{for} \quad y = 1$$

$$V_x = 0, \quad V_y = -1, \quad T = \frac{T_0}{T_1 - T_0} \text{ for } \quad y = -1 \quad (11)$$

The incompressibility of the fluid implies the existence of a stream function ψ which is a physical quantity related to the velocity field and can be defined for different flow configurations. It can be used to compute the flow streamlines corresponding to fluid particle trajectories for a steady flow as it is the case in this work. The stream function related to the velocity components is defined in order to satisfy the continuity Eq. (7) as follows:

$$V_x(x,y) = \frac{\partial \psi}{\partial y}, \qquad V_y(x,y) = -\frac{\partial \psi}{\partial x} \qquad (12)$$

The purpose of introducing the stream function in the problem is to produce the vorticity transport equation that characterizes the flow under study and is obtained by taking the curl of the momentum equation and by considering the transformation (12). Indeed, due to the existence of the stream function, the governing equations become:

$$\frac{\partial \psi}{\partial x}\frac{\partial}{\partial y}(\Delta\psi) - \frac{\partial \psi}{\partial y}\frac{\partial}{\partial x}(\Delta\psi) = \frac{1}{R}\Delta^2\psi \qquad (13)$$

$$\frac{\partial \psi}{\partial y}\frac{\partial T}{\partial x} - \frac{\partial \psi}{\partial x}\frac{\partial T}{\partial y} = \frac{1}{Pé}\left(\frac{\partial}{\partial x}\left(\kappa\frac{\partial T}{\partial x}\right) + \frac{\partial}{\partial y}\left(\kappa\frac{\partial T}{\partial y}\right)\right) \qquad (14)$$

where $\Delta\psi = \frac{\partial V_x}{\partial y} - \frac{\partial V_y}{\partial x}$. The length of the channel is large compared to its width, this leads to prescribe the stream function per unit length *F*. In fact, the existence of the function *F* is accompanied by a new function θ uniform to the temperature. On the other hand, the complete formulation of the problem requires the functional dependence of the nondimensional thermal conductivity on temperature $\kappa(\theta)$. The following transformations are then considered:

$$\psi(x,y) = xF(y)$$

$$T(x,y) = \theta(y) + \frac{T_0}{T_1 - T_0} \qquad (15)$$

$$\kappa(\theta) = 1 + \gamma\theta$$

The nondimensional parameter γ is a measure of the sensitivity of the thermal conductivity to the variations of temperature. Since $\kappa(\theta)$ is positive in this work, thus $\kappa(\theta) > 0$. Considering the nondimensional temperature range by referring to the boundary conditions (11) and the similarity transformations (15): $\frac{T_0}{T_1 - T_0} \le T \le \frac{T_1}{T_1 - T_0}$, this means that $0 \le \theta \le 1$. It follows that $\gamma > -1$. In fact, the thermal conductivity can increase with temperature; this case corresponds to $\gamma > 0$, while a decrease takes place when $-1 < \gamma < 0$. The case of the constant thermal conductivity corresponds to $\gamma = 0$.

The problem to solve is obtained by introducing the similarity transformations (15) into Eqs. (13) and (14):

$$F^{(4)} + R\left(FF^{(3)} - F^{(1)}F^{(2)}\right) = 0 \qquad (16)$$

$$(1+\gamma\theta)\theta^{(2)} + \gamma(\theta^{(1)})^2 + PéF\theta^{(1)} = 0 \qquad (17)$$

The boundary conditions related to the functions *F* and θ are derived:

$$F^{(1)}(1) = 0, F(1) = -1, \quad \theta(1) = 1$$

$$F^{(1)}(-1) = 0, F(-1) = 1, \quad \theta(-1) = 0 \qquad (18)$$

with $F^{(i)} = d^iF/dy^i$ and $\theta^{(i)} = d^i\theta/dy^i$. It follows that the problem is reduced to solving a nonlinear two-point boundary-value problem (16)-(18). By introducing the similarity properties (15) into Eqs. (8) and (9), the pressure terms which have disappeared while taking the curl of the momentum equation, can now be yielded:

$$A = \frac{1}{x}\frac{\partial p}{\partial x} = \frac{1}{R}F^{(3)} + FF^{(2)} - \left(F^{(1)}\right)^2 = \text{constant} \qquad (19)$$

$$Q(y) = \frac{\partial p}{\partial y} = -\frac{1}{R}F^{(2)} - FF^{(1)} \quad (20)$$

At a given Reynolds number, the axial pressure gradient per unit length A as defined in Eq. (19) is constant inside the channel since it is equivalent to the integral of the left hand side of Eq. (16), while the normal pressure gradient Q is defined in Eq. (20).

The differential equations and boundary conditions obtained describe the flow between two parallel porous walls fixed at different temperatures. The porosity of the walls is incorporated in this work as it is taken into account in other studies, especially those which deal with the model of the processes such as the boundary layer separation with suction or injection [29] and filtration [30, 31]. In the absence of the porosity of the walls, this flow configuration is similar to the well known plane Poiseuille flow [32], that is the flow between two parallel solid walls. It is important to note that the original Poiseuille problem that concerned the movement of a fluid in a cylindrical tube has been extended to the flow of a fluid between two parallel planes. As the porous walls can help to model some processes such as the boundary layer separation and filtration, the solid wall cases are applied in some industrial flows to relate, in the same Poiseuille law, the viscosity of the fluid, the flow rate, the pressure difference in the flow and the geometric characteristics of a cylindrical conduit [32]. On the other hand, the Poiseuille flow occurring between two solid planes is usually applied to relate the mean velocity of the flow, the fluid viscosity, the pressure gradient in the flow and the distance between the two planes [32].

3. Description of the numerical integration

In light of Eqs. (16) and (17), the problem provides an analytical solution for the control parameters R, $Pé$ and γ tending to zero. When the control numbers of the problem are not close to zero, Eqs. (16) and (17) are nonlinear. The shooting method associated with the fourth-order Runge-Kutta algorithm is applied to obtain the solution of the nonlinear boundary-value problem (16)–(18). To start, Eqs. (16)-(17) are expressed in the classic form:

$$F^{(4)} = f(y, F, F^{(1)}, F^{(2)}, F^{(3)}) = R(F^{(1)}F^{(2)} - FF^{(3)}) \quad (21)$$

$$\theta^{(2)} = \phi(y, F, \theta, \theta^{(1)}) = -\left(\gamma(\theta^{(1)})^2 + PéF\theta^{(1)}\right)/(1+\gamma\theta) \quad (22)$$

In order to transform the two-point boundary-value problem (16)-(18) into an initial value problem, three new variables a, b and c are introduced as user-specified initial guesses at $y = -1$ as follows:

$$F(-1) = 1,\ F^{(1)}(-1) = 0,\ F^{(2)}(-1) = a,$$
$$F^{(3)}(-1) = b,\ \theta(-1) = 0,\ \theta^{(1)}(-1) = c \quad (23)$$

Thus, the solution of the problem becomes dependent upon four variables y, a, b, c. As permitted by the chain rule, the order of differentiation in Eqs. (21) and (22) can be switched such that:

$$\frac{\partial}{\partial a}\left(f(y, F, F^{(1)}, F^{(2)}, F^{(3)})\right) = \frac{\partial}{\partial a}\left(\frac{\partial^4 F}{\partial y^4}\right) = \frac{\partial^4}{\partial y^4}\left(\frac{\partial F}{\partial a}\right) \quad (24)$$

$$\frac{\partial}{\partial b}\left(f(y, F, F^{(1)}, F^{(2)}, F^{(3)})\right) = \frac{\partial^4}{\partial y^4}\left(\frac{\partial F}{\partial b}\right) = \frac{\partial}{\partial b}\left(\frac{\partial^4 F}{\partial y^4}\right) \quad (25)$$

$$\frac{\partial}{\partial a}\left(\phi(y, F, \theta, \theta^{(1)})\right) = \frac{\partial}{\partial a}\left(\frac{\partial^2 \theta}{\partial y^2}\right) = \frac{\partial^2}{\partial y^2}\left(\frac{\partial \theta}{\partial a}\right) \quad (26)$$

$$\frac{\partial}{\partial b}\left(\phi(y, F, \theta, \theta^{(1)})\right) = \frac{\partial}{\partial b}\left(\frac{\partial^2 \theta}{\partial y^2}\right) = \frac{\partial^2}{\partial y^2}\left(\frac{\partial \theta}{\partial b}\right) \quad (27)$$

$$\frac{\partial}{\partial c}\left(\phi(y, F, \theta, \theta^{(1)})\right) = \frac{\partial}{\partial c}\left(\frac{\partial^2 \theta}{\partial y^2}\right) = \frac{\partial^2}{\partial y^2}\left(\frac{\partial \theta}{\partial c}\right) \quad (28)$$

It can be observed that the function F is independent of c because Eqs. (21) and (22) are solved in partial coupling. More precisely, Eq. (21) does not need any parameter of Eq. (22) to be solved. However, the solution of Eq.

(21) is required in order to achieve the results of Eq. (22). Five new functions *u*, *v*, *g*, *q* and *w* are introduced as follows:

$$u(y,a,b)=\frac{\partial F}{\partial a},\quad v(y,a,b)=\frac{\partial F}{\partial b},$$
$$g(y,a,b,c)=\frac{\partial \theta}{\partial a},\ q(y,a,b,c)=\frac{\partial \theta}{\partial b},\qquad (29)$$
$$w(y,a,b,c)=\frac{\partial \theta}{\partial c}$$

Fourth-order differential equations for *u* and *v* can be derived, and second-order differential equations for *g*, *q* and *w* are obtained from Eqs. (24)-(28) in the form:

$$\frac{\partial^4}{\partial y^4}\left(\frac{\partial F}{\partial a}\right)=\frac{\partial^4 u}{\partial y^4}=\frac{\partial f}{\partial y}\frac{\partial y}{\partial a}+\frac{\partial f}{\partial F}\frac{\partial F}{\partial a}+\frac{\partial f}{\partial F^{(1)}}\frac{\partial F^{(1)}}{\partial a}$$
$$+\frac{\partial f}{\partial F^{(2)}}\frac{\partial F^{(2)}}{\partial a}+\frac{\partial f}{\partial F^{(3)}}\frac{\partial F^{(3)}}{\partial a}\qquad (30)$$

$$\frac{\partial^4}{\partial y^4}\left(\frac{\partial F}{\partial b}\right)=\frac{\partial^4 v}{\partial y^4}=\frac{\partial f}{\partial y}\frac{\partial y}{\partial b}+\frac{\partial f}{\partial F}\frac{\partial F}{\partial b}+\frac{\partial f}{\partial F^{(1)}}\frac{\partial F^{(1)}}{\partial b}$$
$$+\frac{\partial f}{\partial F^{(2)}}\frac{\partial F^{(2)}}{\partial b}+\frac{\partial f}{\partial F^{(3)}}\frac{\partial F^{(3)}}{\partial b}\qquad (31)$$

$$\frac{\partial^2}{\partial y^2}\left(\frac{\partial \theta}{\partial a}\right)=\frac{\partial^2 g}{\partial y^2}=\frac{\partial \phi}{\partial y}\frac{\partial y}{\partial a}+\frac{\partial \phi}{\partial F}\frac{\partial F}{\partial a}+\frac{\partial \phi}{\partial \theta}\frac{\partial \theta}{\partial a}$$
$$+\frac{\partial \phi}{\partial \theta^{(1)}}\frac{\partial \theta^{(1)}}{\partial a}\qquad (32)$$

$$\frac{\partial^2}{\partial y^2}\left(\frac{\partial \theta}{\partial b}\right)=\frac{\partial^2 q}{\partial y^2}=\frac{\partial \phi}{\partial y}\frac{\partial y}{\partial b}+\frac{\partial \phi}{\partial F}\frac{\partial F}{\partial b}+\frac{\partial \phi}{\partial \theta}\frac{\partial \theta}{\partial b}$$
$$+\frac{\partial \phi}{\partial \theta^{(1)}}\frac{\partial \theta^{(1)}}{\partial b}\qquad (33)$$

$$\frac{\partial^2}{\partial y^2}\left(\frac{\partial \theta}{\partial c}\right)=\frac{\partial^2 w}{\partial y^2}=\frac{\partial \phi}{\partial y}\frac{\partial y}{\partial c}+\frac{\partial \phi}{\partial F}\frac{\partial F}{\partial c}+\frac{\partial \phi}{\partial \theta}\frac{\partial \theta}{\partial c}$$
$$+\frac{\partial \phi}{\partial \theta^{(1)}}\frac{\partial \theta^{(1)}}{\partial c}\qquad (34)$$

The variable *y* is independent of *a*, *b*, *c*. On the other hand, the function *F* is independent of *c*, then $\frac{\partial y}{\partial a}=0$, $\frac{\partial y}{\partial b}=0$, $\frac{\partial y}{\partial c}=0$, and $\frac{\partial F}{\partial c}=0$. Equations (30)-(34) become:

$$u_{yyyy}=f_F u+f_{F^{(1)}}u_y+f_{F^{(2)}}u_{yy}+f_{F^{(3)}}u_{yyy}\qquad (35)$$

$$v_{yyyy}=f_F v+f_{F^{(1)}}v_y+f_{F^{(2)}}v_{yy}+f_{F^{(3)}}v_{yyy}\qquad (36)$$

$$g_{yy}=\phi_F u+\phi_\theta g+\phi_{\theta^{(1)}}g_y\qquad (37)$$

$$q_{yy}=\phi_F v+\phi_\theta q+\phi_{\theta^{(1)}}q_y\qquad (38)$$

$$w_{yy}=\phi_\theta w+\phi_{\theta^{(1)}}w_y\qquad (39)$$

where $u_y=\frac{\partial u}{\partial y}$, $u_{yy}=\frac{\partial^2 u}{\partial y^2}$, $u_{yyy}=\frac{\partial^3 u}{\partial y^3}$,

$u_{yyyy}=\frac{\partial^4 u}{\partial y^4}$, $v_y=\frac{\partial v}{\partial y}$, $v_{yy}=\frac{\partial^2 v}{\partial y^2}$, $v_{yyy}=\frac{\partial^3 v}{\partial y^3}$,

$v_{yyyy}=\frac{\partial^4 v}{\partial y^4}$, $g_y=\frac{\partial g}{\partial y}$, $g_{yy}=\frac{\partial^2 g}{\partial y^2}$, $q_y=\frac{\partial q}{\partial y}$,

$q_{yy}=\frac{\partial^2 q}{\partial y^2}$, $w_y=\frac{\partial w}{\partial y}$, $w_{yy}=\frac{\partial^2 w}{\partial y^2}$, $f_F=\frac{\partial f}{\partial F}$,

$f_{F^{(1)}}=\frac{\partial f}{\partial F^{(1)}}$, $f_{F^{(2)}}=\frac{\partial f}{\partial F^{(2)}}$, $f_{F^{(3)}}=\frac{\partial f}{\partial F^{(3)}}$,

$\phi_F=\frac{\partial \phi}{\partial F}$, $\phi_\theta=\frac{\partial \phi}{\partial \theta}$, and $\phi_{\theta^{(1)}}=\frac{\partial \phi}{\partial \theta^{(1)}}$.

To satisfy the endpoint boundary conditions at *y* = 1, the following function *G* needs to be minimized:

$$G(a,b,c)=\left(F(1,a,b)+1\right)^2+\left(F^{(1)}(1,a,b)^2-0\right)^2$$
$$+\left(\theta(1,a,b,c)-1\right)^2\qquad (40)$$

An algorithm for calculating the zeros *a**, *b**, *c** of Eq. (40) can be implemented. The algorithm requires updating the initial guesses as follows:

$$\begin{bmatrix}a\\b\\c\end{bmatrix}_{m+1}=\begin{bmatrix}a\\b\\c\end{bmatrix}_m-[J]^{-1}.\begin{bmatrix}F(1,a,b)+1\\F^{(1)}(1,a,b)-0\\\theta(1,a,b,c)-1\end{bmatrix}_m\qquad (41)$$

where *m* is the iteration index and $[J]^{-1}$ is the inverted Jacobian matrix. The Jacobian itself is defined as:

$$J = \begin{bmatrix} \frac{\partial f_1}{\partial a} & \frac{\partial f_1}{\partial b} & \frac{\partial f_1}{\partial c} \\ \frac{\partial f_2}{\partial a} & \frac{\partial f_2}{\partial b} & \frac{\partial f_2}{\partial c} \\ \frac{\partial \phi_1}{\partial a} & \frac{\partial \phi_1}{\partial b} & \frac{\partial \phi_1}{\partial c} \end{bmatrix}$$
$$= \begin{bmatrix} u(1,a,b) & v(1,a,b) & 0 \\ u_y(1,a,b) & v_y(1,a,b) & 0 \\ g(1,a,b,c) & q(1,a,b,c) & w(1,a,b,c) \end{bmatrix} \quad (42)$$

where $f_1 = F(1, a, b)+1$, $f_2 = F^{(1)}(1,a,b) - 0$ and $\phi_1 = \theta(1,a,b,c) - 1$.

Considering Eqs. (29), the initial conditions corresponding to the differential equations satisfied by the functions u and g are:

$$\begin{aligned} &u(-1,a,b) = 0 \\ &u_y(-1,a,b) = 0 \\ &u_{yy}(-1,a,b) = 1 \\ &u_{yyy}(-1,a,b) = 0 \\ &g(-1,a,b,c) = 0 \\ &g_y(-1,a,b,c) = 0 \end{aligned} \quad (43)$$

while the differential equations verified by the functions v and q are solved subject to the following initial conditions:

$$\begin{aligned} &v(-1,a,b) = 0 \\ &v_y(-1,a,b) = 0 \\ &v_{yy}(-1,a,b) = 0 \\ &v_{yyy}(-1,a,b) = 1 \\ &q(-1,a,b,c) = 0 \\ &q_y(-1,a,b,c) = 0 \end{aligned} \quad (44)$$

On the other hand, the differential equation satisfied by the function w is solved considering the initial conditions:

$$w_y(-1,a,b,c) = 1 \quad (45)$$

At this stage, it appears that the differential Eqs. (16) and (17) with boundary conditions (18) are transformed into seven coupled ordinary differential Eqs. (21), (22), (35)-(39) with initial conditions (23), (43)-(45). The initial value problem is solved using the fourth-order Runge-Kutta integration by assigning twenty variables to represent F, θ, u, g, v, q, w and their respective derivatives as follows:

$$\mathbf{Y} = \left[F \;\; F^{(1)} \;\; F^{(2)} \;\; F^{(3)} \;\; \theta \;\; \theta^{(1)} \;\; u \;\; u_y \;\; u_{yy} \;\; u_{yyy} \right.$$
$$\left. g \;\; g_y \;\; v \;\; v_y \;\; v_{yy} \;\; v_{yyy} \;\; q \;\; q_y \;\; w \;\; w_y \right]^{\mathrm{T}} \quad (46)$$

The associated initial conditions are given as:

$$\mathbf{Y}(-1) = \left[1 \;\; 0 \;\; a \;\; b \;\; 0 \;\; c \;\; 0 \;\; 0 \;\; 1 \;\; 0 \;\; 0 \;\; 0 \;\; 0 \;\; 0 \;\; 0 \;\; 1 \right.$$
$$\left. 0 \;\; 0 \;\; 0 \;\; 1 \right]^{\mathrm{T}} \quad (47)$$

To summarize, since three of the six auxiliary conditions (18) are of the boundary value type, the numerical solution becomes dependent upon three initial guesses a, b and c. To derive the solutions, the two-point boundary-value problem which consists of the ordinary differential Eqs. (16) and (17) with boundary conditions (18) governed by the single variable y is transformed in order to be described by four variables that are the three guesses a, b, c and y. More precisely, it is important to note that the described numerical method is devoted to solving a two-point boundary-value problem transformed into an initial value problem equivalent itself to a resulting set of twenty coupled first-order ordinary differential equations with three unspecified start-up conditions. In seeking the successful initial guesses a^*, b^*, c^*, an optimization type problem is solved.

It is important to note that the shooting method associated with the fourth-order Runge-Kutta algorithm is a rapidly converging numerical approach that many scientists are

making increasing use for solving two-point boundary-value problems, such that some scientists consider the solutions obtained as exact [14, 23, 25].

Equations (12)-(15) derive from a technique using the stream function to solve the differential Eqs. (7)-(10) with the boundary conditions (11). This technique is similar to the Berman approach [11] which inspired other authors [12-17, 22-24] to find the solutions of the Navier–Stokes equations. However, other methods [3, 8, 21, 33, 34, 35] to solve the Navier–Stokes equations and the energy equation exist. Indeed, another approach could consist to determine the flow field characteristics directly without introducing the stream function. The present work is based on the stream function, since the introduction of the stream function in the governing equations enables to determine different solution branches through which the behaviors of the flow field components are examined.

4. Numerical results and discussion

Due to the nonlinearity of the equations describing the problem, multiple solution branches are determined through which the results are presented in terms of profiles of the velocity and temperature. The streamlines or the fluid particle trajectories are also presented in order to highlight the flow patterns through each of the five solution branches I, I_1, I_1', II and III. More precisely, the results from the numerical integration reveal symmetric solution of types I, II and III, as well as asymmetric solutions of types I_1 and I_1'.

In this study, the ranges of the control numbers of the problem depend on the given solution branch. This criterion is specially related to the Reynolds number which governs the dynamics of the fluid. Indeed, relative to the solutions of types I and II for example, above the value of the Reynolds number R = 25 that gives rise to the flattening of the profiles of the axial velocity per unit length, no other hydrodynamic structure is revealed from the numerical results we obtained. This case could lead to consider R = 25 as the high value of the Reynolds number for these two solution branches. Our desire is to find new hydrodynamic structures by varying the control parameters of the problem. On a given solution branch, when nothing new is found by increasing these control parameters, then we stop the calculation program.

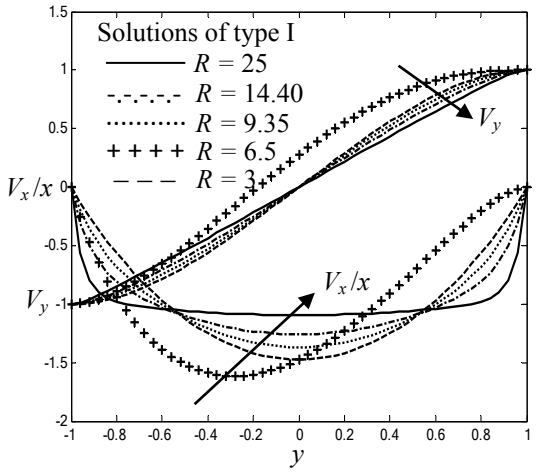

Fig. 2. Axial and normal velocity profiles through the branch I.

4.1 Velocity profiles

The normal velocity V_y and the axial velocity per unit length V_x/x corresponding to solutions of type I are plotted in Fig. 2 which enables to observe that the flow keeps its primary direction $V_x/x < 0$ under different values of R through the branch I. With the growth of the Reynolds number, the function V_x/x increases versus R near the middle of the flow domain, while a decrease occurs in the neighborhood of the walls. Due to this growth of the Reynolds number, the normal velocity tends to satisfy a linear profile of the form $V_y = y$, which is its expected behavior for an inviscid suction flow [22, 23, 36, 37]. In fact, the results from the numerical integration show that, for all the large values of the Reynolds number, the normal velocity and the axial velocity per unit length tend to the same constant curves, respectively. However, for low and moderate values of R through the branch I, while the axial velocity per unit length approaches a parabolic profile, the normal velocity tends to satisfy the Taylor profile given by $\sin(\pi y/2)$ [38].

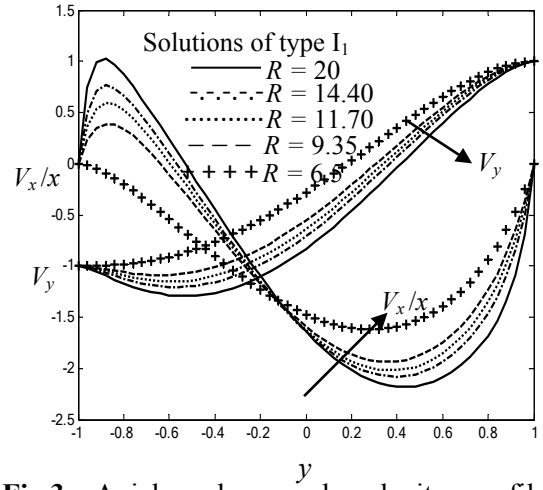

Fig.3. Axial and normal velocity profiles through the branch I_1.

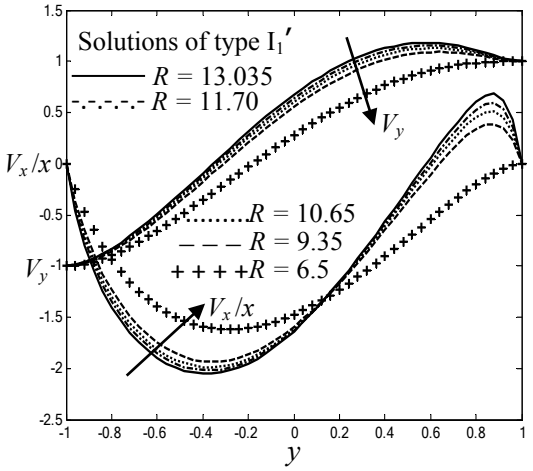

Fig. 4. Axial and normal velocity profiles through the branch I_1'.

The velocity components relative to solutions of type I_1 are presented in Fig. 3 where the axial velocity per unit length shows a region near the lower wall in which the flow does not keep its primary direction; that is a region of flow reversal which is very noticeable with the growth of the Reynolds number and manifests itself as positive values of the function V_x/x. In this region, the magnitude of the normal velocity exceeds its value at walls. Except the neighborhood of the lower wall, in the rest of the channel, the flow keeps its primary direction corresponding to $V_x/x < 0$. It follows that, flow reversal and the primary flow take place concurrently inside the channel through the solution branch of type I_1 in light of Fig. 3.

Inside the channel, the normal velocity corresponding to the branch I_1 decreases with the growth of the Reynolds number according to Fig. 3, while an increase takes place with respect to solutions of type I_1' as shown in Fig. 4 where the reverse flow also known as the backward flow moves from the lower wall to the upper wall. More precisely, the magnitude of the normal velocity corresponding to solutions of type I_1' exceeds its value at walls near the upper wall where flow reversal occurs. It appears that Figs. 3-4 present the opposite behaviors of the velocity components pertaining to the branches I_1 and I_1' within the channel and near the two walls as shown their comparisons in terms of axial velocities per unit length through Fig. 5. These opposite behaviors are due to the fact that, solutions of types I_1 and I_1' behave as mirror images of each other.

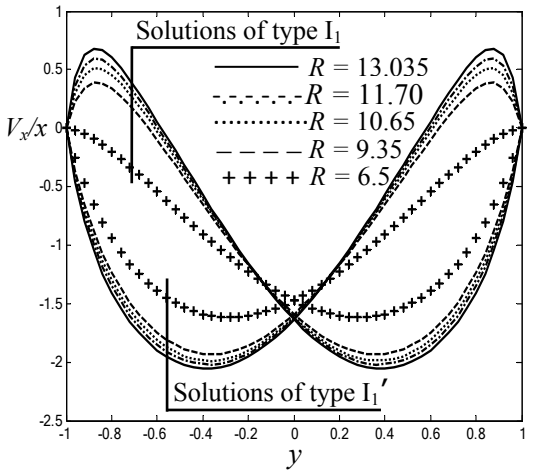

Fig. 5. Comparison of the axial velocities through the branches I_1 and I_1'.

Under different values of the Reynolds number, the normal velocity and the axial velocity profiles through the branch II are plotted in Fig. 6 which reveals the presence of the backward flow around the middle of the flow domain. More precisely, the results from the numerical integration show that the backward flow occurs in the center of the channel through the branch II when the Reynolds number R satisfies the condition

$12.165 < R < 13.119$. As the reverse flow manifests itself near the center of the channel for $12.165 < R < 13.119$ through the branch II, the rest of the channel is characterized by a flow that develops in the primary direction for other values of the Reynolds number according to Fig. 6. Through the branch II, the axial velocity per unit length decreases with the growth of the Reynolds number around the middle of the channel, but increases near the two walls. On the other hand, the normal velocity tends to satisfy an oscillatory profile which is destroyed by the increase in the Reynolds number that gives rise to a linear behavior.

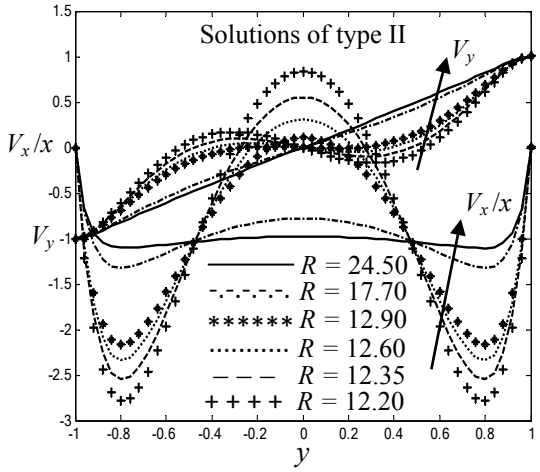

Fig. 6. Axial and normal velocity profiles through the branch II.

The axial velocity per unit length and the normal velocity across the branch III present an oscillatory behavior for all the Reynolds numbers according to Fig. 7 which reveals the existence of a flow that develops in the opposite direction to the primary motion of the fluid near the middle of the channel; while the rest of the flow domain is characterized by the primary motion of the fluid. In Fig. 7, the function V_x/x increases with the Reynolds number near the center of the channel and decreases in the neighborhood of the walls.

4.2 Streamlines

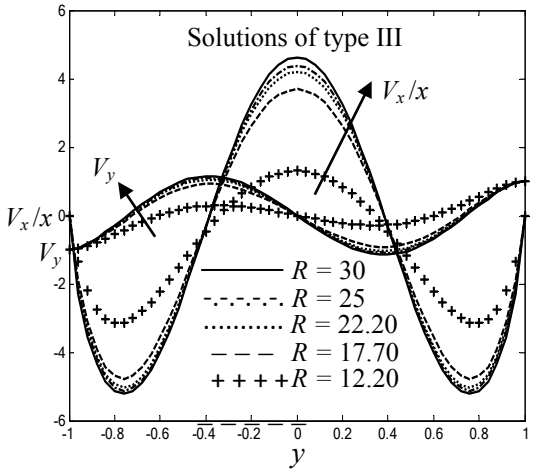

Fig. 7. Axial and normal velocity profiles through the branch III.

The suction-driven flow patterns or the fluid particle trajectories are presented in Fig. 8. The movement of fluid particles corresponding to the branch I for $R = 5.175$ develops in the streamwise direction near the midsection plan considered as an open wall at $y = 0$ and in the normal direction near the walls according to Fig. 8a which shows that the set of the streamlines approaches the walls and moves away from the midsection plane of the flow domain. Relative to the branch I_1, the curvature of the streamlines in the neighborhood of the lower wall is due to the change of direction of the movement because of flow reversal that occurs in this region as presented in Fig. 8b plotted for $R = 13.035$. This curvature of the streamlines deriving from the change of direction due to the backward flow moves from the lower wall to the upper wall in Fig. 8c that represents the flow pattern for $R = 13.035$ corresponding to solutions of type I_1'. The streamlines corresponding to asymmetric solutions of types I_1 and I_1' show that the fluid is not sandwiched inside the channel as in the case of the flow pattern related to symmetric solutions of type I. Indeed, a sandwich flow occurs when the fluid seems to be equally distributed on both sides of the midsection plane of the channel as it is also observed in Fig. 8d which presents the streamlines for $R = 12.645$ belonging to the interval $12.165 < R < 13.119$ where flow

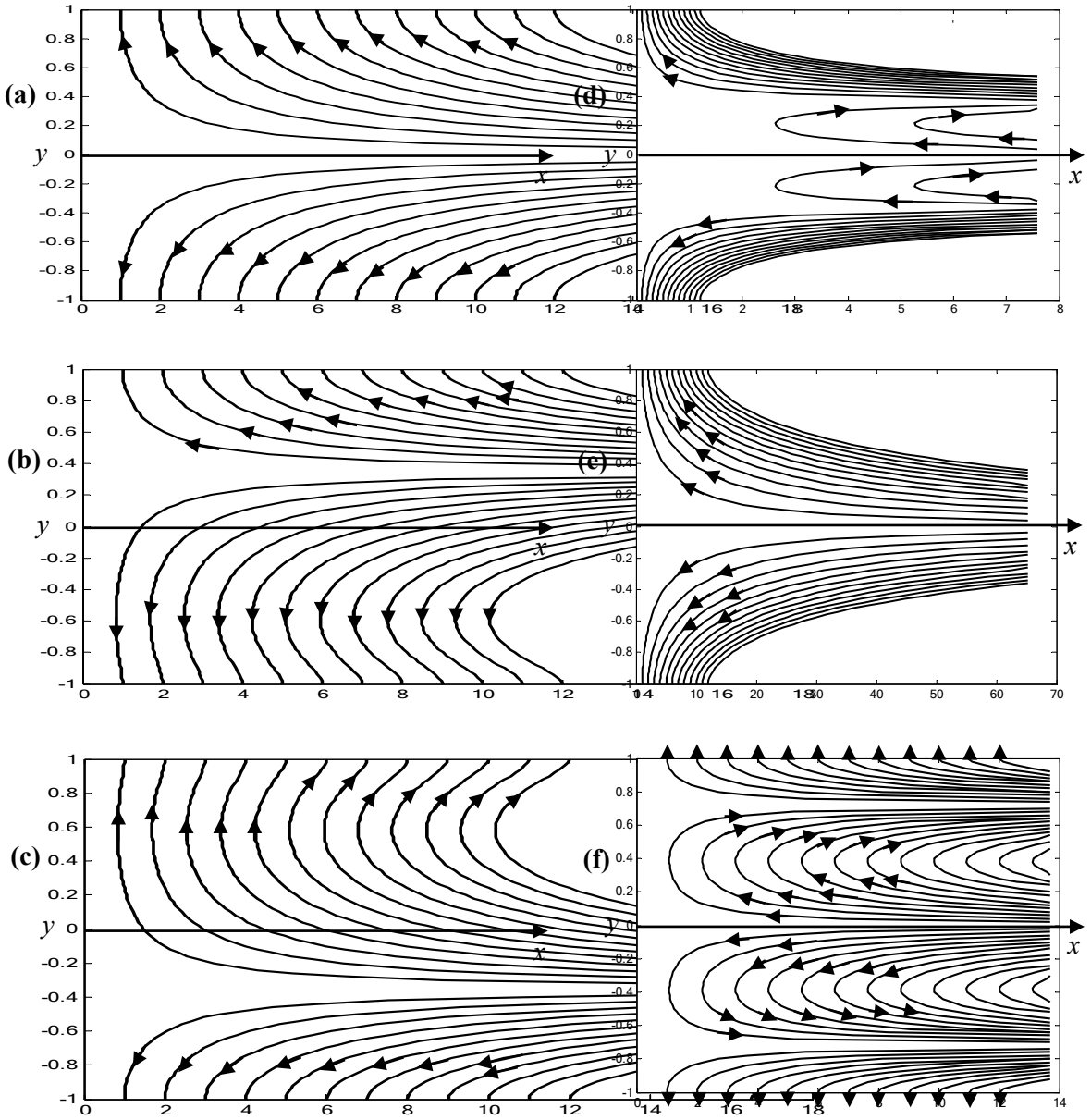

Fig. 8. Streamlines pertaining to (a) the branch I for R = 5.175, (b) the branch I_1 for R = 13.035, (c) the branch I_1' for R = 13.035, (d) the branch II with flow reversal for R = 12.645, (e) the branch II in the absence of flow reversal for R = 14.355, (f) the branch III for R = 17.50.

reversal intervenes and in Fig. 8e for R = 14.355 in the absence of the backward flow through the branch II. Due to the fact that flow reversal takes place on the interval $12.165 < R < 13.119$ around the middle of the channel through the branch II, Fig. 8d obtained for R = 12.645 only shows the curvature of the streamlines around the midsection plane of the flow of the flow domain, while no streamline curvature is observed for R = 14.355 due to the absence of the reverse flow in Fig. 8e. In addition, the set of the streamlines corresponding to the branch II is close to the middle of the channel and far from the walls as shown in Fig. 8 (d, e). Since flow reversal is generalized around the middle of the channel for all the Reynolds numbers through the branch III, the curvature of the streamlines is fully developed in this region in light of Fig. 8f

plotted for R = 17.5. In Fig. 8f the set of the streamlines occupies the maximum volume of the channel.

4.3 Heat transfer patterns

The temperature profiles through the branch I at a fixed Reynolds number, under different Péclet numbers, for positive and negative fixed values of the sensitivity of the thermal conductivity to the variations of temperature are presented in Fig. 9 which shows the existence of a large horizontal inflection area around the middle of the flow domain. This large horizontal inflection area presents two concavities, such that the first concavity located near the cold wall is turned towards the stocking and the second concavity situated in the neighborhood of the hot wall is turned towards the top. This inflection area appears as the Péclet number increases by approaching the value of 10, while the decrease in the Péclet number causes a linear profile of temperature inside the channel. Moreover, the temperature profiles across the branch I present an increase with γ.

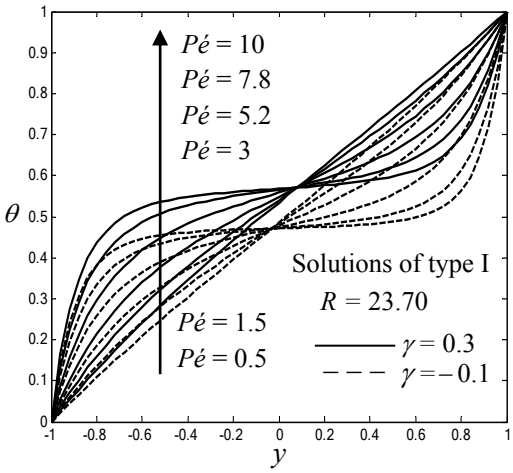

Fig. 9. Temperature profiles through the branch I for R = 23.70.

The increase in the Péclet number by approaching the value of 10 at a fixed Reynolds number, for given negative and positive values of the sensitivity of the thermal conductivity to the variations of temperature causes a growth of temperature towards the upper limit θ = 1 in a large region within the channel by referring to Fig. 10 that exhibits the temperature profiles pertaining to the branch I_1.

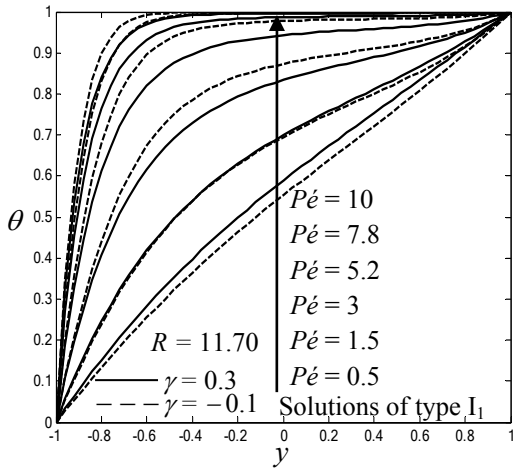

Fig. 10. Temperature profiles through the branch I for R = 23.70.

More precisely, by increasing the Péclet number as shown in Fig. 10, the evolution of temperature begins by a linear law of the form $\theta = y$ to an upper horizontal asymptote given by θ = 1. However, relative to the branch I_1', the increase in $Pé$ close to the value of 10 at a fixed R, for given negative and positive values of the parameter γ causes a decrease of temperature towards the lower limit θ = 0 in a large region within the channel according to Fig. 11. In other words, by increasing the Péclet number as shown in Fig. 11, the behavior of the function θ corresponding to the branch I_1' begins by a linear law of the form $\theta = y$ to a lower horizontal asymptote given by θ = 0. The described thermal behaviors across the branches I_1 and I_1' as shown in Figs. 10-11 reveal the opposite temperature evolutions in the flow domain due to the fact that, the solutions of types I_1 and I_1' behave as mirror images of each other. In fact, the property of mirror images highlighted through the behavior of the velocity components is also encountered relative to the temperature distribution pertaining to the branches I_1 and I_1', because of the influence of the fluid flow on the heat transfer in this study.

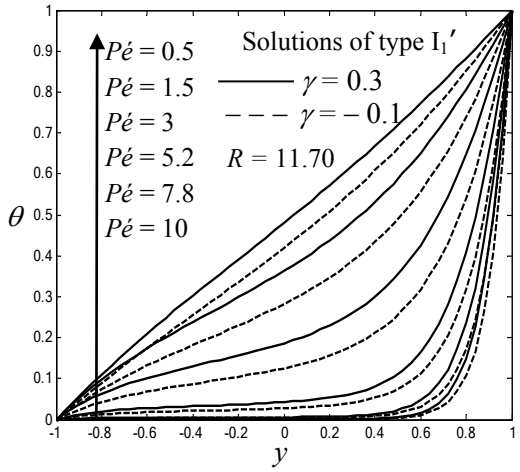

Fig. 11. Temperature profiles through the branch I_1' for $R = 11.70$.

By considering Fig. 12, the temperature distribution relative to the branch II is similar to that of the branch I. Moreover, Fig. 12 enables to observe that the growth in the Reynolds number produces the same effect on temperature like that of the Péclet number across the branch II, this similar effect is the appearance of the inflection area.

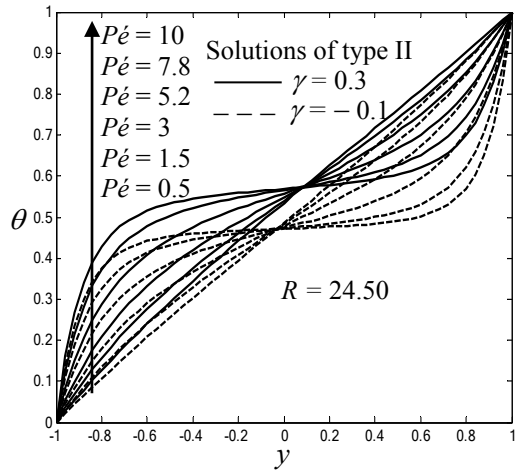

Fig. 12. Temperature profiles through the branch II for $R = 24.50$.

The variation of temperature inside the channel with respect to the branch III reveals the disappearance of the inflection area with the growth of the Péclet number as shown in Fig. 13, but the decrease in *Pé* also causes the linear profile of temperature within the channel as it is found through the other solution branches.

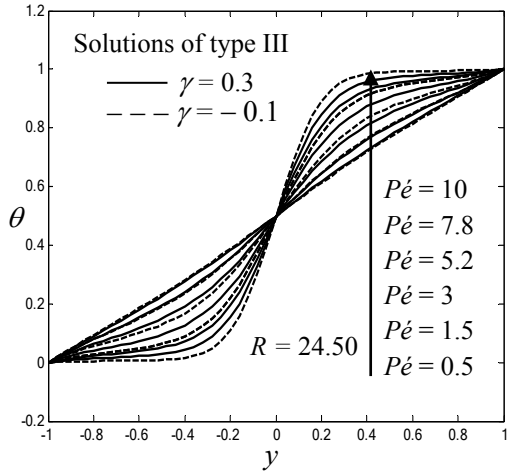

Fig. 13. Temperature profiles through the branch III for $R = 24.50$.

5. Conclusion

The Navier-Stokes equations and the heat transfer equation are used for modeling the fluid flow driven by suction inside a channel that consists of two parallel porous surfaces kept at different temperatures. Due to the incompressibility of the working fluid, the two Navier-Stokes equations are transformed into a single vorticity equation satisfied by the stream function. Then, a similarity method is applied in order to transform the partial differential equations of the problem satisfied by the stream function and temperature into two nonlinear ordinary differential equations describing the same problem. The attention is focused on five solution branches denoted solutions of types I, I_1, I_1', II and III where the dynamics of the fluid and the temperature distribution are investigated under different values of the control parameters of the problem which are the Reynolds number, the Péclet number and the parameter that represents a measure of the sensitivity of the thermal conductivity to the variations of temperature.

The increase in the Reynolds number causes the decrease of the axial velocity per unit length pertaining to solutions of type II around the middle of the channel and an increase near the walls, while the axial velocity per unit length relative to the branch I

increases around the middle of the flow domain and decreases in the neighborhood of the walls. In particular, flow reversal which does not occur for any value of the Reynolds number through the branch I, takes place across the branch II for $12.165 < R < 13.119$, and exists in the middle of the channel for all the values of R across the branch III. For all the Reynolds numbers, as the backward flow does not exist through the branch I, then in this branch the motion of the fluid keeps its primary direction as it is the case near the walls for solutions of types II and III. As solutions of types I_1 and I_1' have regions of flow reversal respectively near the lower wall and the upper wall for the same values of the Reynolds number, they behave as mirror images of each other. In all the cases, when the flow reverses in a given region, a streamline curvature is observed in this respective region inside the channel in order to highlight the fact that the direction of fluid particles changes from the primary to the reverse.

Another attention in this work is focused on the variation of temperature through each solution branch of the two-dimensional channel flow under study. It is found that, the solution branches I and II are characterized by a large inflection area as the Péclet number approaches the value of 10. In addition, the opposite behaviors described between the solutions of types I_1 and I_1' with respect to the velocity components are also raised relative to temperature corresponding to branches I_1 and I_1' due to the influence of the dynamics of the fluid on the heat distribution within the channel.

References

[1] R. Akhter, M.M. Ali, MHD natural convection in nanofluid filled square cavity with isothermally heated hexagonal block, International Journal of Thermofluid Science and Technology 9 (1) (2022) 090104.

[2] M.J. Noroozi, A. Emamifar, A new nonlinear solution for non-Fourier heat transfer in porous fins, International Journal of Thermofluid Science and Technology 8(4) (2021) 080405.

[3] N. Manjunatha, R. Sumithra, R.K. Vanishree, Combined effects of nonuniform temperature gradients and heat source on double diffusive Benard-Marangoni convection in a porous-fluid system in the presence of vertical magnetic field, International Journal of Thermofluid Science and Technology 8(1) (2021) 080104.

[4] M. Abdelkader, H. Ameur, Y. Menni, Investigation of the convective heat transfer and friction factor of magnetic Ni nanofluids within cylindrical pipes, International Journal of Thermofluid Science and Technology 8(1) (2021) 080101.

[5] Y. Belkassmi, L. Elmaimouni, A. Rafiki, K. Gueraoui, N. Hassanain, Heat and mass transfer modeling during laminar condensation of non-cryogenic downward fluids flow in a small vertical tube, International Journal of Thermofluid Science and Technology 7(4) (2020) 070401.

[6] J.J. Wylie, J.R. Lister, The effect of temperature dependent viscosity on flow in a cooled channel with application to basaltic fissure eruption, Journal of Fluid Mechanics (305) (1995) 239-261.

[7] M. A. Hossain, K. Khanafer, K. Vafai, The effect of radiation on free convection flow of fluid with variable viscosity from a porous vertical plate, International Journal of Thermal Sciences 40(2) (2001) 115-124.

[8] N.G. Kafoussius, D.A.S. Rees, J.E. Daskalakis, Numerical study of the combined free-forced convective laminar boundary layer flow past a vertical isothermal flat plate with temperature-dependent viscosity, Acta Mechanica 127(1) (1998) 39-50.

[9] J. Gary, D.R. Kassory, H. Tadjeran, A. Zebib, The effect of significant viscosity variation on convective heat transport in water-saturated porous media, Journal of Fluid Mechanics (117) (1982) 233-249.

[10] H. Ockendon, J. R. Ockendon, Variable viscosity flows in heated and cooled channels, Journal of Fluid Mechanics 83(1) (1977) 177-190.

[11] A. S. Berman, Laminar flow in channels with porous walls, Journal of Applied Physics 24(9) (1953) 1232-1235.

[12] J. F. Brady, Flow development in a porous channel or tube, Physics of Fluids 27(5) (1984) 1061-1067.

[13] M.B. Zaturska, P.G. Drazin, W.H.H. Banks, On the flow of a viscous fluid driven along a channel by suction at porous walls, Fluid Dynamics Research 4(3) (1988) 151-178.

[14] S.M. Cox, Two-dimensional flow of a viscous fluid in a channel with porous walls, Journal of Fluid Mechanics (227) (1991) 1-33.

[15] J. Hona, E. Ngo Nyobe, E. Pemha, Numerical investigation of high viscous fluid flow between two porous plates using the shooting technique, International Journal of Engineering Systems Modelling and Simulation 7(3) (2015) 192-201.
[16] V. Nyemb Nsoga, J. Hona, E. Pemha, Numerical simulation of heat distribution with temperature-dependent thermal conductivity in a two-dimensional liquid flow, International Journal of Nonlinear Sciences and Numerical Simulation 18(6) (2017) 507-513.
[17] S. Ferro, G. Gnavi, Effects of temperature-dependent viscosity in channels with porous walls, Physics of Fluids 14(2) (2002) 839-849.
[18] M.L. Martins-Costa, R.M. Saldanha Da Gama, S. Frey, Modeling of a generalized Newtonian flow through channels with permeable walls, Mechanics Research Communications 27(6) (2000) 707-712.
[19] E. Magyari, B. Keller, Exact solutions for self-similar boundary-layer flows induced by permeable stretching walls, European Journal of Mechanics B Fluids 19(1) (2000) 109-122.
[20] E.B.B. Watson, W.H.H. Banks, M.B. Zaturska, P.G. Drazin, On transition to chaos in two-dimensional channel flow symmetrically driven by accelerating walls, Journal of Fluid Mechanics (212) (1990) 451-485.
[21] S. Xinhui, Z. Liancun, Z. Xinxin, Y. Jianhong, Homotopy analysis method for the heat transfer in an asymmetric porous channel with an expanding or contracting wall, Applied Mathematical Modelling 35(9) (2011) 4321-4329.
[22] C. Zhou, J. Majdalani, Improved mean-flow solution for slab rocket motors with regressing walls, Journal of Propulsion and Power 18(3) (2002) 703-711.
[23] C.E. Dauenhauer, J. Majdalani, Exact self-similarity solution of the Navier–Stokes equations for a porous channel with orthogonally moving walls, Physics of Fluids 15(6) (2003) 1485-1495.
[24] J. Hona, E. Ngo Nyobe, E. Pemha, Dynamic behavior of a steady flow in an annular tube with porous walls at different temperatures, International Journal of Bifurcation and Chaos 19(9) (2009) 2939-2951.
[25] W.H.H. Banks, M.B. Zaturska, On flow through a porous annular pipe, Physics of Fluids A 4(6) (1992) 1131–1141.
[26] T. Saad, J. Majdalani, Viscous mean flow approximations for porous tubes with radially regressing walls, AIAA Journal 55(11) (2017) 3868-3880.
[27] J. Griffond, G. Casalis, On the dependence on the formulation of some nonparallel stability approaches applied to the Taylor flow, Physics of Fluids 12(2) (2000) 466-468.
[28] J. Griffond, G. Casalis, On the nonparallel stability of the injection induced two-dimensional Taylor flow, Physics of Fluids 13(6) (2001) 1635-1644.
[29] G. Raithby, Laminar heat transfer in the thermal entrance region of circular tubes and two-dimensional rectangular ducts with wall suction and injection, International Journal of Heat and Mass Transfer 14(2) (1971) 223-242.
[30] M.-M. Kim, A.L. Zydney, Theoretical analysis of particle trajectories and sieving in a two-dimensional cross-flow filtration system, Journal of Membrane Science 281(1-2) (2006) 666-675.
[31] Z. Jalilvand, F.Z. Ashtiani, A. Fouladitajar, H. Rezaei, Computational fluid dynamics modeling and experimental study of continuous and pulsatile flow in flat sheet microfiltration membranes, Journal of Membrane Science (450) (2014) 207-214.
[32] W.C. Chin, More steady flow applications, In: Managed Pressure Drilling: Modelling, Strategy, and Planning, Waltham: Gulf Professional Pub., 2012.
[33] R. Hiptmair, L. Li, S. Mao, W. Zheng, A fully divergence-free finite element method for magnetohydrodynamic equations, Mathematical Models and Methods in Applied Sciences 28(4) (2018) 659-695.
[34] N. Bildik, A. Konuralp, The use of variational iteration method, differential transform method and Adomian decomposition method for solving different types of nonlinear partial differential equations, International Journal of Nonlinear Sciences and Numerical Simulation 7(1) (2006) 65-70.
[35] W.F. Ames, Numerical solutions of partial differential equations, In: Academic Press, Second Edition, New York, 1977.
[36] R.M. Terrill, Laminar flow in a uniformly porous channel, Aeronautical Quarterly 15(3) (1964) 299-310.
[37] J.R. Sellars, Laminar flow in channels with porous walls at high suction Reynolds numbers, Journal of Applied Physics 26(4) (1955) 489-490.
[38] G.I. Taylor, Fluid flow in regions bounded by porous surfaces, Proceedings of the Royal Society of London 234(1199) (1956) 456-475.